Proceedings of the ASME 2017 Pressure Vessels and Piping Division Conference
PVP2017
July 16-20, 2017, Waikoloa Village, Hawaii, United States

PVP2017-65857

HYDROGEN ISOTOPE PERMEATION AND TRAPPING IN ADDITIVELY MANUFACTURED STEELS

Richard A. Karnesky
Sandia National Laboratories
Livermore, CA, USA

Paul Chao
Carnegie Mellon University
Pittsburgh, PA, USA

Dean A. Buchenauer
Sandia National Laboratories
Livermore, CA, USA

ABSTRACT

Additively manufactured (AM) austenitic stainless steels are intriguing candidates for the storage of gaseous hydrogen isotopes. Complex vessel geometries can be built more easily than by using conventional machining options. Parts built with AM steel tend to have excellent mechanical properties (with tensile strength, ductility, fatigue crack growth, and fracture toughness comparable to or exceeding that of wrought austenitic stainless steel). However, the solidification microstructures produced by AM processing differ substantially from the microstructures of wrought material. Some features may increase permeability, including both some amount of porosity and a greater amount of ferrite. Because the diffusivity of hydrogen in ferrite is greater than in austenite (six orders of magnitude at ambient temperature), care must be taken to retain the performance that is taken for granted due to the base alloy chemistry. Furthermore, AM parts tend to have greater dislocation densities and greater amounts of carbon, nitrogen, and oxygen. These features, along with the austenite/ferrite interfaces, may contribute to greater hydrogen trapping.

We report the results of our studies of deuterium transport in various austenitic (304L, 316, and 316L) steels produced by AM (via either powder bed fusion or blown powder methods). The hydrogen permeability (an equilibrium property) changes negligibly (less than a factor of 2), regardless of chemistry and processing method, when tested between 150 and 500 °C. This is despite increases in ferrite content up to FN=2.7. However, AM materials exhibit greater hydrogen istotope trapping, as measured by permeation transients, thermal desorption spectra, and inert gas fusion measurement. The trapping energies are likely modest (<10 kJ/mol), but may indicate a larger population of trap sites than in conventional 300-series steels.

INTRODUCTION

Additively-manufactured (AM) metals, particularly those made from austenitic stainless steel powder that is melted with a laser, have been proposed for both building new parts [1] and for repairing damaged parts [2–4] for hydrogen service. While both of these use-cases are proposed to take advantage of AM's unique abilities to build to complex (and even conformal) geometries, the material selected for the powder is not novel to the process. Conventionally-manufactured austenitic stainless steel is resistant to hydrogen-assisted fracture [5–7] and has a reasonably modest permeability for hydrogen isotopes at typical operating temperatures and pressures [8].

However, the solidification microstructures of AM austenitic steels differ from conventionally-proceesed microstructures. The grain size is fine (d~10-100 μm [9–11]). Although wrought or worked (e.g. rolled) material may also have d<100 μm [12,13], the grain structure of AM materials tends to be different. AM materials tend to have elongated grains (aspect ratios of 2-3:1) and are more highly textured. Due to their rapid solidification, AM austenitic stainless steels tend to retain more δ-ferrite than conventional materials (FN<6, though some still routes lead to levels below detection limits [14]). The initial dislocation density tends to be very high (ρ~2.4×10^{14} m^{-2} [15] vs. ρ~10^{12} m^{-2} for wrought [12]). The chemistry of the AM parts depends not only on the composition of the starting powder (which tends to have greater amounts of N and O) and the build environment (inert Ar, typically), but also on interactions with the laser, which may change the chemistry of the bulk part from the powder due to preferential vaporizing. For example, the level of N in parts built from virgin powder is typically about 0.04 wt.% [9], though building in inert N drives this to about 0.5 wt.% [16]). The distribution of elements within a built part is expected to be different because of the high solidification rate, though limited high resolution studies have been done to date. Finally, the porosity of AM built parts tends to be slightly higher due to closed pores in the starting powder and lack-of-fusion defects.

These microstructural differences between AM and conventional materials lead to differences in properties. The literature typically reports greater yield strengths in AM steels, for example [1,9,10,14,15]. The different microstructure may also lead to a difference in how hydrogen isotope transport through AM materials. Porosity and ferrite, for example, may

conceivably increase permeability over that of a fully austenitic conventional material (ferrite has a hydrogen permeability that is six orders of magnitude larger than austenite's at ambient temperature) [17]. However, we're not aware of any other effort to characterize hydrogen isotope permeability of AM materials and, with the exception of the letter by Baek *et al.* [1], there seems to be no effort to characterize hydrogen isotope trapping to the defects enumerated above.

This study explores hydrogen isotope transport in AM austenitic stainless steels through gas-driven permeation and thermal desorption of hydrogen isotope-charged specimens. A number of AM builds are explored here in order to determine the extent to which AM processing changes the behavior of hydrogen in the material. Future studies will probe the microstructural origins for these changes.

MATERIALS AND METHODS

The materials in this study are listed in Table 1. Initial powder chemistry met the ASTM/SAE specifications for grades 316, 316L, and 304L [18]. All materials started with a different batch of powder and all were built on different machines. We have given the laser energy of the builds where we know them. Some samples were extracted from "plate" or "column" builds, so that we measure permeation through the build layers (z). Some were "wall" or "fin" builds, so that permeation is measured orthogonal to this (x/y).

The Laser Engineered Net Shaping ® (LENS®) process, commercialized by Optomec (Albuquerque, NM), uses Direct Laser Powder Deposition (DLPD). A laser is focused on a metal substrate and metal powder is fed into a flowing argon stream. The laser and powder feeder translate together, the laser melting the deposited powder. The melt pool solidifies while the laser/powder feeder head deposits more material elsewhere on the substrate. In addition to build from standard Optomec machines, one build came from a DLPD machine operating at a much higher laser powder.

In the Powder Bed Fusion (PBF) process (also known as "selective laser melting"), a layer of powder is placed on a substrate, a laser rasters over selected portions of the layer and then a new layer of powder is placed down. In this study, a Renishaw AM 250 was used.

Foils were cut for permeation testing (ca. 2.5 cm in diameter, 0.025-0.05 cm thick) and ground to a 1 μm finish. A Feritscope was used to measure the ferrite content (also given in Table 1) and then the samples were coated with Pd to prevent oxidation. The method of permeability testing is described in Refs. [19,20]. In short: the sample is sandwiched between two copper gaskets in a large VCR-style fitting and the assembly is inserted into a vacuum tube furnace (this outer vacuum preventing any spurious signals from gas that leaks around the sample). The sample is brought to temperature under vacuum. A half atmosphere of deuterium gas is then applied to the upstream side of the sample. Downstream, the a 1-100AMU residual gas analyzer monitors all peaks associated with deuterium.

After the initial measurement at 200 °C, the sample was raised to 300 °C, pumped of any detectable deuterium, and gas was again applied. The testing proceeded in these 100 °C increments until 500 °C. After testing was completed, the sample was left at temperature for deuterium to pump out, and then lowered to 450 °C for testing. This downward ramp was repeated until 250 or 150 °C. Any microstructural changes that may change permeability due to the long time at temperature would be expected to lead to changes between the upward vs. downward temperature ramps.

Similar thickness foils were cut for deuterium- or hydrogen- charging for thermal desorption spectroscopy and inert gas fusion analysis. This charging occurred at 138 MPa, 300 °C for two weeks, ample time to saturate the thin specimens, even with a high expected population of traps [21,22]. Hydrogen-charged samples were submitted to IMR Test Labs (Portland, OR) for Inert Gas Fusion-Infrared Absorbance testing of total hydrogen content. Deuterium-charged samples were tested by thermal desorption spectroscopy, per Ref. [23]. Here, we present 0.05 cm-thick samples heated at a rate of 6 °C/min from room temperature to 800ºC in order to compare with literature testing of conventional 304 [24,25] and 316L [25–27].

FERRITE CONTENT

Ferrite content for all materials was fairly low (FN<3) and, in one case, undetectable with the Feritscope (FN<0.2). The ferrite content did not change significantly after permeation testing. Because part shape, powder chemistry, laser power, and cooling rate all varied build-to-build, we see no trends in ferrite content with any individual process parameter. Chemical composition tends to have a very strong role, though [28,29]. But the higher C expected in LENS1 compared to the builds using 316L did not seem to stabilize any more austenite.

The powders used in builds LENS3 and PBF have similar powder and build chemistry (both: 18.9 Cr, 9.9 Ni, 1.5 Mn, 0.58 Si, 0.05 N (all in wt. %)), although PBF has twice the O content as LENS3 (0.04 wt.% vs. 0.02 wt.%). Higher O is thought to lead to more ferrite [30], counter to the trend of these two builds. The more rapid cooling rate of PBF compared to LENS [31] may have been responsible for a liquid→austenite solidification in PBF in contrast to a liquid→ferrite+austenite solidification/transformation in LENS. But, again: there are a large number of variables and this may be coincidence.

PERMEATION

Hydrogen-equivalent permeabilities (assuming a square root of mass dependence on permeation) are given in Figure 1. The values for the tested AM materials of this study fall within a factor of 2 of that expected for conventional 300-series steels [8], below the spread reported for conventional materials in the literature. Despite the modest ferrite content in the AM material here, the values are not higher than conventional austenitic stainless steel. We've reported a similar trend in 21-6-9 with FN~2, though we've observed higher permeabilities in both 304 autogenous weld material and 2507

duplex steels [19]. The ferrite of the AM materials is expected to be very fine. It is unlikely to be connected in through-thickness "stringers" that would serve as short-circuit diffusion paths, particularly in the "plate" builds here. Any effect of ferrite may also be masked by microstructural features which may reduce permeation (such as the internal oxides, originating from oxide on the surface of the starting powder).

Activation energies calculated from data in Figure 1 are given in Table 2. These are in reasonable agreement with those for conventionally processed 300-series stainless steels.

The permeability is the equilibrium product of the diffusivity and the solubility. Our experiments also measure the deuterium flux transients, from which an apparent diffusivity can be extracted. Figure 2 depicts the transient for DLPD at 200 °C A Fourier fit shows the apparent diffusivity is two orders of magnitude lower than is expected in conventional 300-series steels. This is likely due to trapping at microstructural defects.

HYDROGEN ISOTOPE CONTENT AND TRAPPING

Thermal desorption spectra are given in Figure 3. Integrating these curves gives the total amount of deuterium desorbed from the samples. Table 3 presents the average hydrogen isotope content for the materials over all desorption run and from inert gas fusion analysis (we assume here that the solubility and trapping are independent of isotope). The errors given are a single standard deviation from the mean. With the exception of the PBF material, all were within a single deviation of the concentration expected from the charging conditions and the solubility for hydrogen isotopes in convention 300-series steels. However, all means were as high or slightly higher than that value. This slight excess may be due to hydrogen isotopes trapped at microstructural defects that we inferred in the previous section from Figure 2.

Conventional 300-series steels tend to have very low concentrations of trapped hydrogen (unless they're deformed to produce α-martensite) and the traps tend to have a very low influence on hydrogen transport due to (i) the very low binding energies associated with traps; (ii) the relatively high diffusivity for hydrogen in austenite; and (iii) the relatively low solubility for hydrogen in austenite [8,32–35].

But multiple distinct peaks observed in desorption spectra here also support our finding that there's a greater amount of trapping in AM material. Detailed analysis of the trapping is confounded: we consider only a single thermal ramp rate and the materials have many processing/microstructural differences and the shape of some peaks do not appear to be what would be expected from first-order desorption. Based on peak locations at this single ramp rate, we observed no desorption energies greater than ca. 64 kJ/mol, no higher than energies measured for tritium desorption [36]. Considering that the activation energy for hydrogen diffusion is austenite is 54 kJ/mol [8], this corresponds to trap binding energies that are less than 10 kJ/mol, somewhat lower than the 15 kJ/mol vacancy binding energy [25–27,37] and the unidentified 19 kJ/mol traps in Ref. [38]. It is also *much* lower than the binding energy found for trap sites created by ion implantation [39,40].

Although austenite/ferrite interfaces have been shown to trap hydrogen [41], the amount of trapped hydrogen here does not correlate to the measured ferrite content. Carbide precipitates have also been identified as a possible trap source [42]. All starting powders in this study except for LENS1 had a low nominal C content. While C may be on the powder surface or picked up in the build environment, the LENS3 build has 0.008 wt.% C and PBF has 0.012 wt.% C, both within specification[18]. The estimated binding energies for these AM materials are lower than those attributed to carbides and nitrides. It seems that the most likely explanation for the increased trapping is an increase in the density of sites that exist in conventional 300-series steels, such as vacancies and/or dislocations. However, further studies are needed to better elucidate this.

The results here differ from Baek, *et al.*'s findings [1], which found slightly less hydrogen in AM 304L than in rolled 304L and did not identify any other trapping peaks. The samples there were charged with only 10 MPa H_2 at 150 °C for 5 days. We have four possible explanations for discrepancies between our findings and theirs: (i) based on our permeation transients, 5 days may not have been enough time to saturate the specimens in their study; (ii) their lower charging pressure and temperatures leads to a lower concentration of trapped hydrogen, which may be difficult to detect; (iii) they terminated their experiments at 600 °C, apparently near the beginning of a second peak; or (iv) there may be microstructural differences between our samples that would lead to differences in trapping.

CONCLUSIONS

This study of hydrogen isotope transport in five different AM builds leads to the following conclusions:

- AM processing leads to very different microstructures than conventional processing of 300-series stainless steels, including but not limited to a higher typical ferrite content (up to ca. FN=2.7).
- Despite microstructural differences, the permeability for hydrogen isotopes in AM 300-series steels is within a factor of 2 of conventional 300-series steels and there is no significant change of activation energy.
- AM-processed steels exhibit a great degree of hydrogen isotope trapping than conventional austenitic steels. The origin has not been determined, but the trapping energies seem to be relatively low. This trapping may lead to slightly elevated retention of hydrogen isotopes.

ACKNOWLEDGMENTS

The authors thank D. Balch, M. Maguire, T. Palmer, C. San Marchi, J. Rodelas, J. Smugeresky, and N. Yang for samples and discussions.

Sandia National Laboratories is a multi-program laboratory managed and operated by Sandia Corporation, a wholly owned subsidiary of Lockheed Martin Corporation, for the U.S. Department of Energy's National Nuclear Security Administration under contract DE-AC04-94AL85000.

REFERENCES

[1] Baek, S.-W., Song, E. J., Kim, J. H., Jung, M., Baek, U. B., and Nahm, S. H., 2017, "Hydrogen Embrittlement of 3-D Printing Manufactured Austenitic Stainless Steel Part for Hydrogen Service," Scr. Mater., **130**, pp. 87–90.

[2] Korinko, P., and Thad Adams, T., 2007, "Hydrogen Effects on Laser Engineered Net Shape (LENS) Repaired Weldments," *8th Global Innovations Symposium: Trends in Materials and Manufacturing Technologies for Energy Production*, J.A. Hines, D.F. Bahr, and J.E. Smugeresky, eds., TMS, Pittsburgh, PA, p. 57.

[3] Korinko, P. S., Adams, T. M., Malene, S. H., Gill, D., and Smugeresky, J., 2011, "Laser Engineered Net Shaping® for Repair and Hydrogen Compatibility," Weld. J., **90**, pp. 171–181.

[4] Korinko, P. S., 2015, "Development of Laser Engineered Net Shape (LENS) Additive Manufacturing for Repair," *ASME 2015 Pressure Vessels and Piping Conference*, ASME, Boston, p. V06AT06A003.

[5] Caskey, G. R., 1985, "Hydrogen Effects in Stainless Steel," *Hydrogen Degradation of Ferrous Alloys*, R.A. Oriani, J.P. Hirth, and M. Śmiałowski, eds., Noyes Publications, Park Ridge, N.J., pp. 822–862.

[6] Louthan, M. R., Caskey, G. R., Donovan, J. A., and Rawl, D. E., 1972, "Hydrogen Embrittlement of Metals," Mater. Sci. Eng., **10**, pp. 357–368.

[7] San Marchi, C., and Somerday, B. P., 2012, *Technical Reference for Hydrogen Compatibility of Materials*, SAND2012-7321, Sandia National Laboratories, Livermore, CA.

[8] San Marchi, C., Somerday, B. P., and Robinson, S. L., 2007, "Permeability, Solubility and Diffusivity of Hydrogen Isotopes in Stainless Steels at High Gas Pressures," Int. J. Hydrog. Energy, **32**(1), pp. 100–116.

[9] Wang, Z., Palmer, T. A., and Beese, A. M., 2016, "Effect of Processing Parameters on Microstructure and Tensile Properties of Austenitic Stainless Steel 304L Made by Directed Energy Deposition Additive Manufacturing," Acta Mater., **110**, pp. 226–235.

[10] Yadollahi, A., Shamsaei, N., Thompson, S. M., and Seely, D. W., 2015, "Effects of Process Time Interval and Heat Treatment on the Mechanical and Microstructural Properties of Direct Laser Deposited 316L Stainless Steel," Mater. Sci. Eng. A, **644**, pp. 171–183.

[11] Trelewicz, J. R., Halada, G. P., Donaldson, O. K., and Manogharan, G., 2016, "Microstructure and Corrosion Resistance of Laser Additively Manufactured 316L Stainless Steel," JOM, **68**(3), pp. 850–859.

[12] Venugopal, S., Mannan, S. L., and Prasad, Y. V. R. K., 1994, "Processing Maps for Hot Working of Commercial Grade Wrought Stainless Steel Type AISI 304," Mater. Sci. Eng. A, **177**(1), pp. 143–149.

[13] Venugopal, S., Mannan, S. L., and Prasad, Y. V. R. K., 1992, "Processing Map for Cold and Hot Working of Stainless Steel Type AISI 304 L," Mater. Lett., **15**(1), pp. 79–83.

[14] de Lima, M. S. F., and Sankaré, S., 2014, "Microstructure and Mechanical Behavior of Laser Additive Manufactured AISI 316 Stainless Steel Stringers," Mater. Des., **55**, pp. 526–532.

[15] Clausen, B., Brown, D. W., Carpenter, J. S., Bernardin, J. D., Spernjak, D., Thompson, J. M., Adams, D. P., Reedlunn, B., Carroll, J. D., and Palmer, T. A., 2016, *Using* in Situ *Neutron to Probe the Microstructure of Additively Manufactured Materials during Processing*, LA-UR-16-21394, Los Alamos National Laboratory, Los Alamos, NM.

[16] Conde, A., García, I., and de Damborenea, J. J., 2001, "Pitting Corrosion of 304 Stainless Steel after Laser Surface Melting in Argon and Nitrogen Atmospheres," Corros. Sci., **43**(5), pp. 817–828.

[17] Causey, R. A., Karnesky, R. A., and San Marchi, C., 2012, "Tritium Barriers and Tritium Diffusion in Fusion Reactors," *Comprehensive Nuclear Materials*, R.J.M. Konings, and R.E. Stoller, eds., Elsevier, Amsterdam, pp. 511–549.

[18] ASTM, 2016, *Standard Specification for Chromium and Chromium-Nickel Stainless Steel Plate, Sheet, and Strip for Pressure Vessels and for General Applications*, A240, ASTM International, West Conshohocken, PA.

[19] Buchenauer, D. A., and Karnesky, R. A., 2015, *Stainless Steel Permeability*, SAND2015-8057R, Sandia National Laboratories, Livermore, CA.

[20] Buchenauer, D. A., Karnesky, R. A., Fang, Z. Z., Ren, C., Oya, Y., Otsuka, T., Yamauchi, Y., and Whaley, J. A., 2016, "Gas-Driven Permeation of Deuterium through Tungsten and Tungsten Alloys," Fusion Eng. Des., **109**–**111**, pp. 104–108.

[21] Baskes, M. I., 1980, *DIFFUSE: A Code to Calculate One-Dimensional Diffusion and Trapping*, SAND-80-8201, Sandia National Laboratories, Livermore, CA.

[22] Hardwick, M. F., and Robinson, S. L., 1998, *DIFFUSE II: A Hydrogen Isotope Diffusion and Trapping Simulation Program Upgrade*, SAND99-8202, Sandia National Laboratories, Livermore, CA.

[23] Chao, P., and Karnesky, R. A., 2016, "Hydrogen Isotope Trapping in Al-Cu Binary Alloys," Mater. Sci. Eng. A, **658**, pp. 422–428.

[24] Todoshchenko, O., Yagodzinskyy, Y., Papula, S., and Hänninen, H., 2014, "Hydrogen Solubility and Diffusion in Metastable Austenitic Stainless Steels Studied with Thermal Desorption Spectroscopy," *Hydrogen-Materials Interactions: Proceedings of the 2012 International Hydrogen Conference*, ASME Press, New York, NY, pp. 615–623.

[25] Todoshchenko, O., 2015, *Hydrogen Effects on Austenitic Stainless Steels and High-Strength Carbon Steels*, Aalto University, Helsinki, Finland.

[26] Ganchenkova, M., Todoshchebko, O., Yagodzinskyy, Y., and Hänninen, H., 2012, "Hydrogen Solubility and Trapping in AISI 316L Austenitic Stainless Steel," *Hydrogen-Materials Interactions: Proceedings of the*

2012 International Hydrogen Conference, ASME Press, New York, NY, pp. 605–613.
[27] Todoshchenko, O., Yagodzinskyy, Y., and Hänninen, H., 2013, "Thermal Desorption of Hydrogen from AISI 316L Stainless Steel and Pure Nickel," Defect Diffus. Forum, **344**, pp. 71–77.
[28] Schaeffler, A. L., 1974, "Constitution Diagram for Stainless-Steel Weld Metal," Met. Prog., **106**(1), pp. 227–227.
[29] DeLong, W. T., Ostrom, G. A., and Szumachowski, E. R., 1956, "Measurement and Calculation of Ferrite in Stainless Steel Weld Metal," Weld. J., **35**(11), p. 4.
[30] Ferrante, M., and Farrar, R. A., 1982, "The Role of Oxygen Rich Inclusions in Determining the Microstructure of Weld Metal Deposits," J. Mater. Sci., **17**(11), pp. 3293–3298.
[31] Frazier, W. E., 2014, "Metal Additive Manufacturing: A Review," J. Mater. Eng. Perform., **23**(6), pp. 1917–1928.
[32] Thomas, G. J., 1980, "Hydrogen Trapping in FCC Metals," *Hydrogen Effects in Metals: Proceedings of the Third International Conference on Effect of Hydrogen on Behavior of Materials*, I.M. Bernstein, and A.W. Thompson, eds., Metallurgical Society of AIME, Warrendale, PA, pp. 77–85.
[33] Mine, Y., Horita, Z., and Murakami, Y., 2010, "Effect of High-Pressure Torsion on Hydrogen Trapping in Fe–0.01 Mass% C and Type 310S Austenitic Stainless Steel," Acta Mater., **58**(2), pp. 649–657.
[34] Louthan, M. R., and Derrick, R. G., 1975, "Hydrogen Transport in Austenitic Stainless Steel," Corros. Sci., **15**(6), pp. 565–577.
[35] Wilson, K. L., and Baskes, M. I., 1978, "Thermal Desorption of Deuterium-Implanted Stainless Steel," J. Nucl. Mater., **74**(1), pp. 179–184.
[36] Hirabayashi, T., Saeki, M., and Tachikawa, E., 1984, "A Thermal Desorption Study of the Surface Interaction between Tritium and Type 316 Stainless Steel," J. Nucl. Mater., **126**(1), pp. 38–43.
[37] Myers, S. M., Wampler, W. R., and Besenbacher, F., 1984, "Trapping and Surface Recombination of Ion-implanted Deuterium in Stainless Steel," J. Appl. Phys., **56**(6), pp. 1561–1571.
[38] Yagodzinskyy, Y., Todoshchenko, O., Papula, S., and Hänninen, H., 2011, "Hydrogen Solubility and Diffusion in Austenitic Stainless Steels Studied with Thermal Desorption Spectroscopy," Steel Res. Int., **82**(1), pp. 20–25.
[39] Bohdansky, J., Wilson, K. L., Pontau, A. E., Haggmark, L. G., and Baskes, M. I., 1980, "Combined Depth Profiling and Thermal Desorption of Implanted Deuterium in 304LN Stainless Steel," J. Nucl. Mater., **93**, pp. 594–600.
[40] Wilson, K. L., and Baskes, M. I., 1978, "Deuterium Trapping in Irradiated 316 Stainless Steel," J. Nucl. Mater., **76–77**, pp. 291–297.
[41] Luppo, M. i, Hazarabedian, A., and Ovejero-García, J., 1999, "Effects of Delta Ferrite on Hydrogen Embrittlement of Austenitic Stainless Steel Welds," Corros. Sci., **41**(1), pp. 87–103.
[42] Bacher, J.-P., Benvenuti, C., Chiggiato, P., Reinert, M.-P., Sgobba, S., and Brass, A.-M., 2003, "Thermal Desorption Study of Selected Austenitic Stainless Steels," J. Vac. Sci. Technol. A, **21**(1), pp. 167–174.

Table 1. Materials

ID	Powder	Process	Geometry	Ferrite
LENS1	316	LENS-0.325 kW	Wall	1.1
LENS2	316L	LENS-0.5 kW	Plate	0.3
LENS3	304L	LENS	Wall	0.9
DLPD	304L	DLPD-3.8kW	Plate	2.7
PBF	304L	PBF	Plate	<0.2

Table 2. Activation energies determined by permeation.

ID	Activation energy [kJ/mol]
Conventional [8]	59.8
LENS1	60±2
LENS2	65±2
DLPD	57±2

Table 3. Hydrogen isotope content after gas-charging 140MPa H_2 or D_2 at 300 °C.

ID	Hydrogen isotope content [wt. ppm]*
Conventional [8]	140
LENS1	160±30
LENS3	150±20
DLPD	140±20
PBF	170±20

* H-equivalent concentration given by dividing D concentration by 2

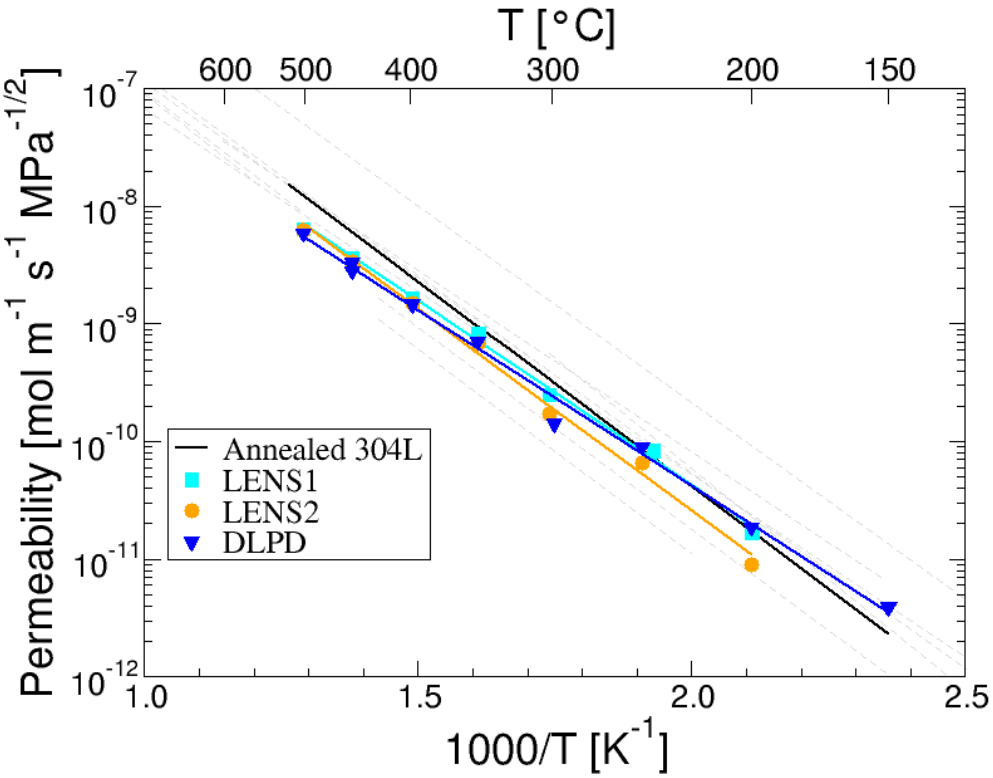

Figure 1. Permeability of various AM steels.

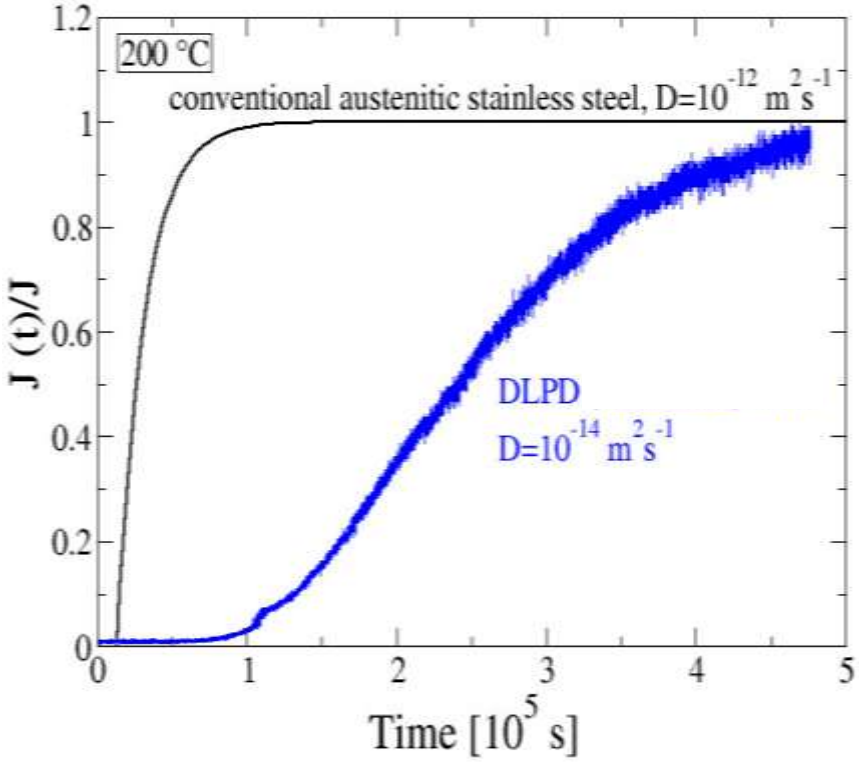

Figure 2. The permeation transient shows that it takes much longer for a DLPD steel to achieve steady-state permeation in comparison to conventional steel. This is indicative of trapping.

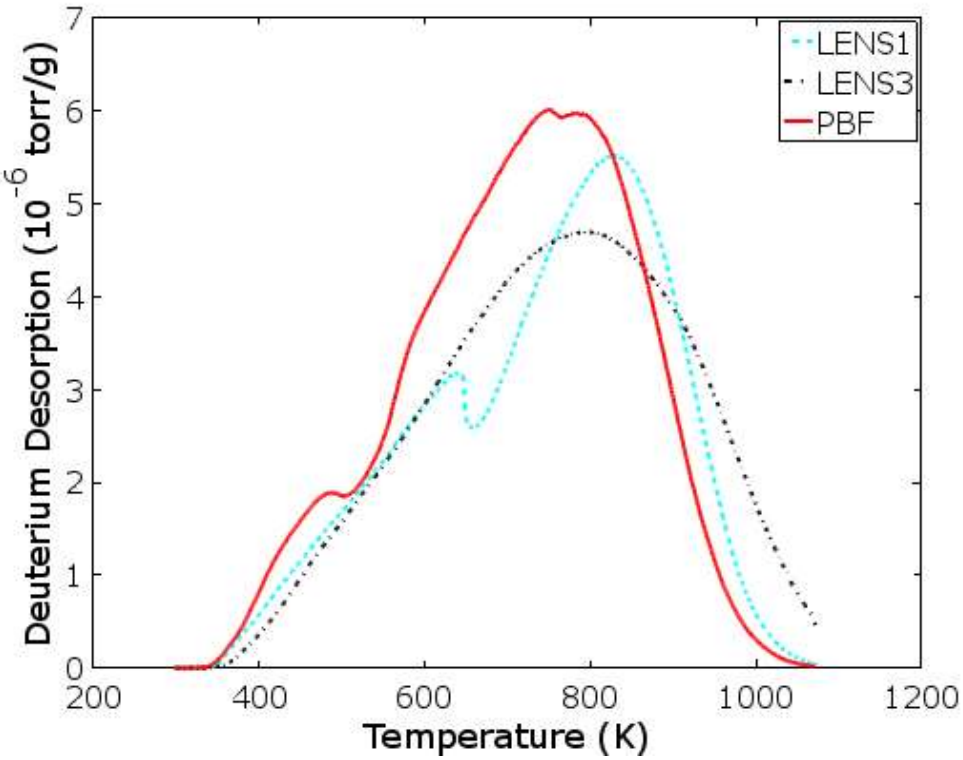

Figure 3. Thermal desorption spectra of charged samples heated 6 °C/min.